6104 *Biochemistry* **2009,** *48,* 6104–6110
DOI: 10.1021/bi900351m

BIOCHEMISTRY
including biophysical chemistry & molecular biology
Article

CO Photodissociation Dynamics in Cytochrome P450BM3 Studied by Subpicosecond Visible and Mid-Infrared Spectroscopy[†]

Alisa Rupenyan,[‡] Jan Commandeur,[§] and Marie Louise Groot*[,‡]

[‡]*Department of Physics and Astronomy, Faculty of Sciences, VU University Amsterdam, Amsterdam, The Netherlands, and* [§]*Department of Pharmacochemistry, Faculty of Sciences, VU University Amsterdam, Amsterdam, The Netherlands*

Received March 2, 2009; Revised Manuscript Received May 27, 2009

ABSTRACT: Cytochrome P450BM3 is a bacterial enzyme with a heme cofactor that binds small diatomic ligands. Here we report the first study of carbon monoxide (CO) photodissociation and rebinding in ferrous P450BM3 on an ultrafast time scale. We monitored dissociation of carbon monoxide upon Soret band excitation using visible and infrared femtosecond spectroscopy between 100 fs and 4 ns. The dynamics of the ferric P450 was probed for reference in the visible spectral region. In the photodissociated ferrous P450−CO complex, the vibrational hot deligated ground state is populated in 0.2 ps and relaxes on a picosecond time scale. The onset of geminate recombination of CO with the heme is observed on a nanosecond time scale. In the mid-infrared spectral region, the bleached absorption due to the bound C=O stretch vibration is constant on the picosecond to 1 ns time scale, indicating that the photodissociation yield is 100% and that rebinding occurs after 1 ns. In the infrared absorption difference spectra, we additionally resolve two small bands of dissociated CO molecules at 2092 and 2114 cm^{-1}. This indicates that the escape of photolyzed CO to solvent and the geminate recombination are preceded by transient docking within the protein in a manner similar to that of globins. The bands partially decay with a time constant of 1 ps, possibly due to a relaxation of the protein around the CO docking site, allowing for greater orientational freedom of the CO molecules.

Cytochrome P450s are a widely distributed family of heme enzymes (*1*) involved in numerous biological processes, which include the biosynthesis of lipids, steroids (*2*), and antibiotics and the degradation of xenobiotics (*3*, *4*). The main catalytic function of P450 proteins is the transfer of one oxygen atom from molecular oxygen to lipophilic substrates. For this monooxygenase reaction, cytochrome P450s receive electrons from NADPH or NADH via electron transfer proteins (*5*). The spectral properties of P450 suggest that it is a ferric hemoprotein with a thiolate group as the fifth axial Fe heme ligand (*1*, *6*).

The use of a cysteine (thiolate) residue as a ligand to the heme is a particular structural feature in P450 (*1*, *7*). Histidine is the overwhelming choice for heme proteins as their proximal ligand. It is found in cytochromes, globins, oxygen sensors such as FixL, and other heme proteins. However, to accomplish the activation of molecular oxygen (O−O cleavage), a strong electron-donating proximal ligand like cysteine (in its anionic form) is needed in P450 (*7*).

Cytochrome P450BM3 (CYP102A1) catalyzes hydroxylation of saturated and monounsaturated fatty acids, alcohols, and amides at the ω-1, ω-2, and ω-3 positions (*8*). It is catalytically self-sufficient P450, having a heme-containing domain and a FAD- and FMN-containing redox domain (*9*). Its structure is known from X-ray crystallography studies and, together with the structures of other bacterial P450s, provides a template for modeling and for elucidation of the role of the conserved residues (*10*) in eukaryotic P450s playing a crucial role in drug metabolism. X-ray diffraction studies demonstrate an open channel within the protein, proposed to be a substrate channel, which closes upon substrate binding (*11*). The active site becomes inaccessible to solvent predominantly because of changes in the orientation of the F- and G-helices forming an amino acid lid of the closed substrate-binding pocket. It has been proposed that different protein funnels open and close to accommodate the substrate and the molecular oxygen within the protein (*12*).

Diatomic heme ligands like carbon monoxide, dioxygen, and nitric oxide have been used as molecular probes for protein dynamics in heme proteins such as hemoglobin (Hb), myoglobin (Mb) (*13*−*17*), FixL (*18*), and nitric oxide reductase (*19*) (for a recent review, see ref (*20*)). The heme Fe−CO[1] bond is broken with high quantum efficiency upon electronic excitation of the heme, rapidly generating a nonequilibrium state within the protein whose relaxation can be monitored experimentally. In globins, photolysis of the CO−Fe bond is followed by release of the CO molecule to the solvent and concomitant relaxation of the

[†]This work was supported by The Netherlands Organization for Scientific Research (NWO-ALW).

*To whom correspondence should be addressed. E-mail: ML.Groot@few.vu.nl. Phone: +31-(0)20-598 2570. Fax: +31-(0)20-598 7999.

[1]Abbreviations: CO, carbon monoxide; OD, optical density; au, arbitrary units; EADS, evolution-associated difference spectra; FTIR, Fourier transform infrared; Mb, myoglobin; IR, infrared.

Published on Web 06/03/2009

surrounding protein (*21*). Deligated CO follows a defined trajectory through the protein to the solvent via several internal protein binding sites (*19*, *21*). These sites are hydrophobic in nature and have been termed xenon sites for their propensity to bind a xenon atom (*22*). In Mb, the deligated CO stays for several nanoseconds in the first binding site, having different orientations toward the heme plane(*23*). Recent molecular dynamics simulations in Mb find two discrete pathways for CO migration in the protein matrix (*24*), and CO escape rates in line with vibrational time-resolved spectroscopy results (*25*). Several substrate transport channels and a putative gaseous ligand entry channel have been identified in the crystal structures of P450s using molecular dynamics simulations (*26*−*28*). In P450cam, a soluble P450 protein, four xenon binding sites were found, two of them highly occupied by xenon atoms, lined by lysine, alanine, and isoleucine residues (*29*).

CO rebinding to P450BM3 was studied from the nanosecond to millisecond time scales by flash photolysis (*30*, *31*). In the absence of the substrate, 30% of the CO ligands rebind geminately to the heme on a nanosecond time scale. The addition of a substrate increases the geminate yield to ~50% (*31*). High-pressure stopped-flow studies of carbon monoxide and molecular oxygen binding to the heme domain of P450BM3 provide evidence that the oxygen binding to P450BM3 occurs via the same mechanism as CO binding with similar rate constants (*32*).

We present the first picosecond visible pump mid-infrared probe and visible pump visible probe spectroscopy study of the heme domain of the bacterial enzyme cytochrome P450BM3 complexed with CO to reveal the dynamics associated with the escape of CO from the heme into the protein and the solvent. Transient absorption of the heme chromophore, and changes in the oscillator strength and stretch frequency of CO, reporting on changes in the interaction between free CO and its protein/solvent environment, have been monitored spectroscopically from 150 fs to 3 ns after photolysis of the CO.

MATERIALS AND METHODS

Protein Purification. The purification of cytochrome P450BM3 (*Bacillus megaterium*) heme domain was performed following ref (*33*) with some modifications. Cultures were grown in LB (Luria-Bertani) medium with 0.3 mg/mL kanamycin at 37 °C and shaken at 150 rpm overnight. Expression of P450BM3 was initiated by the addition of 2 mM IPTG (isopropyl β-D-thiogalactopyranoside). Cells were harvested after 4 h and pelleted by centrifugation (15 min at 4000*g* and 4 °C). The resulting pellet was resuspended in 100 mM potassium phosphate buffer (pH 7.5), with 0.1 mM phenylmethanesulfonyl fluoride (PMSF) to minimize proteolysis. After the addition of 0.1 mg/mL lysozyme, the cells were disrupted using a French press twice (6.9 MPa), and the insoluble parts were removed by centrifugation (60 min at 120000*g* and 4 °C). The supernatant was incubated, while being gently rocked, with Ni-NTA (nickel-nitrilotriacetic acid) agarose for 30 min at 4 °C, and the column material was retained in a polypropylene tube with a porous disk (Pierce) and washed with KP_i buffer containing 2 mM L-histidine. Subsequently, P450 was eluted with 0.3 M L-histidine. After overnight dialysis in KP_i buffer, the sample was concentrated on a Vivaspin 20 filtration tube (10000 MWCO PES, Sartorius). P450 contents were determined by monitoring the CO (carbon monooxide) difference spectra (*34*).

The ferrous (CO) complexes were prepared by adding a few microliters of a 2 mM deaerated dithionite solution, to reduce the heme, and bubbling the protein solution with CO gas for 1−2 min. The sample was deoxygenated prior to reduction by purging N_2 gas in the protein solution for 2 min. Reduction and CO binding were controlled by following the absorption change of the solution. Samples consisted of a highly concentrated protein solution in 100 mM potassium phosphate buffer (pH 7.5) contained between two CaF_2 windows, separated by a 120 μm Teflon spacer. The concentration of the sample was 0.8 mM.

Ultrafast Spectroscopy. The experimental setup consists of an integrated Ti:sapphire oscillator-regenerative amplifier laser system (Hurricane, SpectraPhysics, Mountain View, CA) operating at 1 kHz and at a central wavelength of 800 nm, producing 85 fs pulses of 0.55 mJ. Part of this 800 nm light was used to pump a noncollinear optical parametric amplifier in which a CaF_2 plate was used for white light generation of the seed (*35*) to produce the excitation pulses with a center wavelength of 465 nm and an energy of 300 nJ. A second portion of the 800 nm light was used to pump an optical parametric generator and amplifier with a difference frequency generator (TOPAS, Light Conversion, Vilnius, Lithuania) to produce the mid-IR probe pulses. These low-intensity probe pulses were spatially overlapped with the excitation beam in the sample, which was focused to a diameter of approximately 120−150 μm, and a slightly smaller diameter was used for the probe pulses. After overlap in the sample had been achieved, the mid-IR probe pulses were dispersed in a spectrograph and imaged onto a 32-element MCT detector (Infrared Associates, Orlando, FL). The polarization of the excitation pulse was set to the magic angle (54.7°) with respect to the IR probe pulses. A phase-locked chopper, operating at 500 Hz, ensured that the sample was excited every other shot, and an absorbance difference spectrum could be calculated. To ensure a fresh spot for each laser shot, the sample was moved by a homebuilt Lissajous scanner. The measurements were performed in a box flushed with dry air to reduce the interference of water vapor with the measurements. In a single experiment, a spectral probe window of ~200 cm^{-1} was covered. Measurements in the spectral region of 1860−2140 cm^{-1} were performed with a resolution of ~9 cm^{-1} and repeated twice in three overlapping spectral windows with a resolution of 4 cm^{-1}. One measurement typically consisted of 30−60 scans (termed one data set), in which 80 time points (average of 500 laser shots per point) were collected. The data were subjected to global analysis (*36*). An extra component in the analysis of the mid-IR data accounted for cross-phase modulation and other coherent interactions of the pump and probe pulse around time zero. For each spectral window, the resulting evolution-associated difference spectra (EADS) with similar time constants were averaged. Because of the presence of a perturbed free induction decay before time zero, no information faster than the instrument response (~180 fs) was extracted. Absorption changes in spectral windows containing bands associated with bound CO (1900−2045 cm^{-1}) and photolyzed CO (2077−2180 cm^{-1}) were recorded. The averaged EADS have been drawn with a spline function to represent more realistic spectral bands.

The vis−vis experiments were performed with the same setup (*37*), which was extended with an arm in which white light was generated in a 2 mm CaF_2 plate. This probe light was focused on the sample with the same lens used to focus the excitation pulse, dispersed on a spectrograph, and imaged onto one of the arrays of a double 256-element diode array (Hamamatsu Photonics, Hamamatsu, Japan). The diode array was read after every shot using a 16-bit ADC (Analogue Device) and EDT CD 20

digital I/O board. The instrument response function was ~110 fs in the visible and ~150 fs in the mid-IR experiments. For the vis−vis experiment, the excitation wavelength was set at 465 nm (P450−CO complex), or 400 nm (oxidized P450), and the excitation energy was the same as in the vis-pump−IR-probe experiments.

The amino acid sequences of P450BM3 (PDB entry 2IJ2) and P450cam (PDB entry 1UYU) were aligned with ClustalW2. Cavity search in P450BM3 was performed with CASTp (*38*) (polar hydrogens were removed prior to calculation). Structure representations were made with PyMol (De Lano Scientific LLC, San Carlos, CA).

RESULTS

Steady State Spectra. The normalized steady state spectra of oxidized (Fe^{3+}), reduced (Fe^{2+}), and CO-complexed P450BM3 (Fe^{2+}−CO) are shown in Figure 1A, together with the Fe^{2+} minus CO-complexed P450 difference spectrum. The Fe^{2+} minus CO-complexed P450 difference spectrum exhibits a bleach of the Soret peak of the CO-complexed form at 448 nm, a bleach of the Q-band at 550 nm, and positive absorption of the Soret peak of the reduced form at 411.5 nm. A small shoulder in the spectrum of the CO-complexed P450 peaking at 423 nm indicates the presence of a small amount of either P420 (the inactive form of P450) or unreduced P450.

Transient Absorption Spectra of P450BM3 in the Visible Region. Absorption changes, induced by excitation of the heme at 465 nm, were recorded in the visible spectral region for both reduced CO-ligated heme and oxidized heme.

The time-dependent spectral evolution of the data collected for CO-complexed P450 (Figure 1B,D) is described well using a simple sequential scheme, with increasing exponential lifetimes of 0.2 ps, 4 ps, and 1 ns and a component that does not decay on the time scale that we probed. A selection of the collected time traces is shown in Figure 1D along with the fit. All evolution-associated difference spectra (EADS) in Figure 1B are characterized by a bleach centered at 448 nm. The initial spectrum (black EADS) shows a small positive band at 410 nm, a shoulder at 423 nm, and a negative signal in the Q-band region, peaking at 542 nm arising from ground state bleach. In the 4 ps EADS (red), we observe a small increase in the amplitude of the bleach at 448 nm, a rise of the signal at 410 nm, and a decay of the negative band at 542 nm. The final EADS (blue), formed after 4 ps, shows a complete disappearance of the 423 nm shoulder and a further increase in the amplitude of the 448 nm negative band and 410 nm product band. This spectrum coincides very well with the difference spectrum of the reduced minus CO-complexed P450 spectrum shown in Figure 1A (thin solid line). Therefore, these experiments show that the deligated ground state is formed mainly in 0.2 ps. The 4 ps minor phase may either indicate a long-lived fraction of excited states or be indicative of a vibrational cooling process occurring on the deligated ground state. Note that 4 ps is a time constant typical for vibrational cooling in heme proteins (*39*−*42*). To characterize the spectral signature of vibrational cooling in excited heme, we measured the absorption changes of oxidized P450.

These data (Figure 1C) show a more multiphasic behavior, requiring four kinetic components for the fit: 0.7, 4, and 370 ps

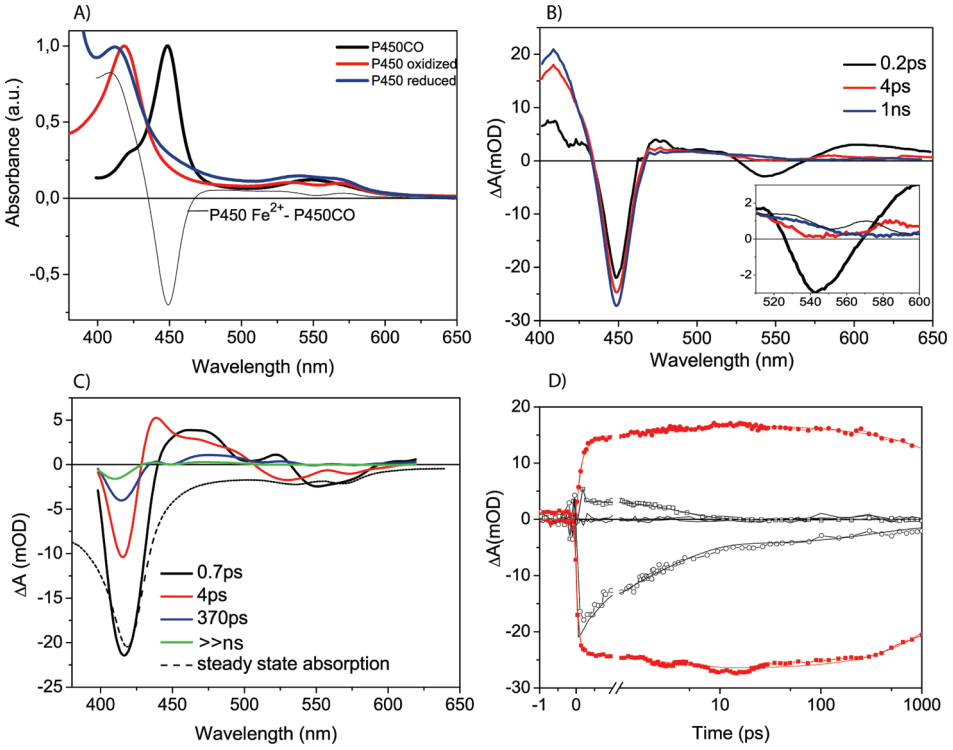

FIGURE 1: Global analysis of the data in the visible spectral region. (A) Steady state spectra of CO-ligated P450 (black line), oxidized (Fe^{3+}) P450 (red line), and reduced (Fe^{2+}) P450 (blue line) and the difference spectrum generated by the subtraction of CO-complexed P450 from the Fe^{2+} P450 (thin solid line). (B) Evolution-associated difference spectra (EADS) representing the kinetics of the CO-ligated heme (solid lines), color-coded according to their decay times (the EADS of the long-lived component is not shown for the sake of clarity, but the 1 ns process accounts for a 10% decay of the signal). The inset zooms in on the spectral region of 510−600 nm (Q-bands), overlaid with the difference spectra of the Fe^{2+}−P450CO complex (thin solid line). (C) EADS representing the kinetics of the unligated heme (solid lines), color-coded according to their decay times, and the steady state absorption spectrum of the unligated Fe^{3+} sample (dashed line). (D) Selected time traces of identical wavelengths for the two samples with fits and residuals derived from global analysis of the data: CO-ligated P450 [447 nm (red squares) and 417 nm (red circles)] and unligated P450 [447 nm (□) and 417 nm (○)]. The fit and the residuals are represented with black solid lines.

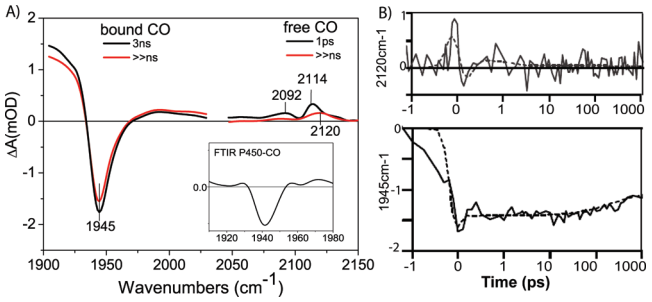

FIGURE 2: Global analysis of the data in the mid-IR spectral region (1900−2150 cm^{-1}). (A) EADS of the P450−CO complex, color-coded according to their decay times. The inset shows the FTIR steady state spectrum of the P450−CO complex in the region of the bound C═O stretch. (B) Time traces corresponding to absorption changes of bound CO (1945 cm^{-1}) and free CO (2120 cm^{-1}) together with fits (dashed lines). The time axis is linear up to 1 ps and logarithmic from 1 to 1000 ps.

and a long-lived component. In the initial EADS (black), the bleach of the Soret band and the Q-bands are present, together with a broad excited state absorption band centered at ~460 nm. After 0.7 ps, the positive band shifts to 436 nm and becomes narrower, and the amplitude and width of the bleached band decrease, indicating overlap with the positive, induced absorption. The subsequent EADS (blue), formed after 4 ps, is characterized by a further recovery of the ground state absorption and a minor broad red-shifted positive absorption. In the final EADS (green), only a small blue-shifted ground state bleach remains. The long lifetime of this state (much greater than nanoseconds) may indicate the presence of a long-lived product state, due to a photoconversion process.

Vibrational Transient Absorption Spectra of Carbon Monoxide. (i) Heme-Bound CO. The maximum absorption change upon excitation of the heme at 465 nm within the 1900−2130 cm^{-1} spectral window (Figure 2A,B) is found at ~1945 cm^{-1}. It coincides with a band in the steady state FTIR absorption spectrum which is only present when CO is bound to the heme (see Figure 2A, inset), in accordance with the frequency of the bound C═O stretch observed by FTIR in P450cam (*43*). The data in the 1900−2030 cm^{-1} region can be fitted with a subpicosecond component, accounting for coherent effects and perturbed free induction decay, and two components with lifetimes of ~1 and ≫3 ns (see Figure 2B for time traces with fits). As we probe only the first 3 ns, we cannot reliably estimate the longer lifetime. The 1 ns component describes a decay of ~10% of the signal amplitude (see Figure 2A,B).

The positive absorption at wavenumbers below 1930 cm^{-1} is due to background absorption change, possibly caused by the heating of water molecules (*44*).

(ii) Photodissociated (free) CO. The stretch frequency of CO upshifts after photolysis of the CO−Fe bond to the 2077−2150 cm^{-1} region of the spectrum. Global analysis (Figure 2A,B) reveals at least two positive bands in this region, centered at 2092 and 2114 cm^{-1}, on top of a broad plateau-like positive band. To fit the data, an additional component with a lifetime of 1 ps was introduced, but the signal-to-noise ratio was not sufficient to resolve the 1 ns component (see Figure 2B for time traces with fits). In the initial spectrum, the amplitude of these bands is higher than in the remaining long-lived spectrum, indicating that loss of free CO or loss of oscillator strength occurs in ~1 ps, and the band centered at 2114 cm^{-1} shifts to the red by 6 cm^{-1}. We also observe a broad positive absorption feature, from 2050 to 2100 cm^{-1}, that largely decays with the same time constant.

DISCUSSION

Heme Relaxation. The data in the 400−600 nm region, reflecting heme relaxation after CO dissociation (Figure 1), are characterized by a fast phase. Most likely, the Fe−CO bond is broken in less than 50 fs (*45*−*47*), faster than our time resolution. A species with a positive absorption band at 410 nm characteristic of unligated (or five-coordinated) heme with a proximal thiolate ligand (see Figure 1B, red spectrum) appears in ~200 fs and remains without major changes until the end of the probe time; only a small increase in the amplitude concomitant with an increase in the bleach is observed in ~4 ps, and a minor decay of 10% after 1 ns.

The 4 ps dynamics may be due to either the decay of a small fraction of excited ferric (unligated) complexes (or P420 complexes) or the blue shifting and narrowing of the product band, as a consequence of cooling of the heme. The steady state absorption spectrum shows that possibly a small fraction of ferric complexes or P420 complexes is present in the sample, and the measured dynamics of excited Fe^{3+} heme reveal that the dynamics occur on the 0.7 and 4 ps time scale, similar to that observed for the ligated complexes. However, the efficiency of excitation at 465 nm of ferric or P420 complexes is probably very low, and the ferric spectroscopic changes cannot account quantitatively for the 4 ps spectral changes in the ligated heme complexes. Therefore, we consider vibrational cooling of the heme as a more likely explanation for the 4 ps process. Specifically, in the difference spectra recorded for unligated heme, we demonstrate that vibrationally hot heme is characterized by red-shifted absorption at ~450 nm, which on a time scale of 0.7 and 4 ps blue-shifts to recover the ground state absorption. The time scale we find here is in good agreement with reports of vibrational cooling in myoglobin, occurring in a few picoseconds (*48*, *49*). Unfortunately, these cooling dynamics interfere with the spectral signatures of ligand rebinding. However, geminate recombination of CO is not likely to occur in less than 4 ps, as judged from experiments with other heme proteins (*18*, *46*). Indeed, the dynamics recorded in the region of the bleached C═O stretch show that no rebinding occurs within 1 ns, suggesting that the yield of CO photodissociation in P450 is 100%. We do note, however, that both in the visible and in the mid-IR transient data, an ~1 ns component, accounting for ~10% signal decay, is required to fit the kinetics. Probably, we resolve here the onset of geminate recombination in P450. Measurements of CO recombination on the 10 ns to millisecond time scale demonstrated that in the absence of the substrate, 30% of the CO ligands rebind geminately to the heme on a 10 ns time scale (*31*). Rebinding on a nanosecond time scale would imply that a portion of the dissociated ligands are stored in docking sites within the protein before recombination. The difference spectra recorded in the mid-IR region indeed reveal the presence of two bands, which we assign to dissociated, docked CO, that persist on the 1 ns time scale.

Photodissociated CO. The magnitude of the bleached bound C═O stretch signal is a monitor for CO rebinding, whereas the frequency shifts of the free CO may yield information about the surroundings of the ligand, indicating possible changes in the temperature of the solvent or rearrangements of the molecules and residues forming the ligand cavity. Within the protein matrix,

the stretching frequencies of both heme-bound and dissociated CO are shifted by the internal electric field acting on the CO dipole (*50*). In ferrous globins, the ligand stretch frequency is usually found to decrease upon binding, which is often explained by the transfer of electron density from the iron d_π orbitals (d_{xz} and d_{yz}) to the antibonding π^* orbitals of the ligand (π backbonding); in P450BM3, we find the frequency to be 1945 cm^{-1}, in agreement with earlier reports of the frequency of the bound C=O stretch observed by FTIR in P450cam (*43*).

A time constant of ~1 ps and a nondecaying component are needed to fit the time traces in the free CO absorption region. Like the observations in other heme proteins, the time zero spectra are characterized by two separate bands, at ~2090 and 2119 cm^{-1}. They are downshifted compared to the free CO stretch in Mb (2120 and 2130 cm^{-1}) (*51*) and in FixL (2116 and 2135 cm^{-1}) (*18*) and of the CO stretch of free CO gas, centered at 2143 cm^{-1} (*52*), indicating stronger interactions with the surroundings. The bands in Mb are termed B_1 and B_2 and reflect the CO molecule docked in the protein matrix in two alternate configurations. They have been proposed to correspond to the same protein pocket occupation of the CO molecule, but in a "head first" or "tail first" orientation, each configuration interacting with its environment in a different way (*53*, *54*). In the IR spectra of P450 (Figure 2A), the low-frequency positive band, corresponding to B_1 (peaking at 2092 cm^{-1}) almost disappears after 1 ps, with a concomitant decrease in the intensity of B_2 (peaking at 2120 cm^{-1}). This originates most likely from a change in the oscillator strength of the free CO due to a conformational relaxation around the docked CO molecule. For the alternative explanation, loss of signal due to a population of CO molecules that escapes the protein into the solvent [CO in the solvent exhibits a broad line width (*55*) and, assuming the integrated oscillator strength is more or less constant, would not be observable in our experiment], the 1 ps time constant seems to be too fast. The conformational relaxation may induce a loosening of the protein pocket around CO on the 1 ps time scale, providing greater rotational freedom for the CO, resulting in a broader line shape that disappears in the background of our signal (*56*). Earlier studies in Mb reported an increase in the magnitude of the signal on the 1.6 ps time scale (*57*). This led Lim et al. (*56*) to suggest that the integrated absorbance of CO is partitioned between the narrow B states and a broad (~90 cm^{-1}) unresolved feature. The increase in the magnitude of the signal in Mb was consequently interpreted to be caused by a relaxation of the protein around CO limiting its orientational freedom. Here, we observe a decrease in the magnitude of the signal, and following the same line of reasoning, we suggest a loosening of the protein around the CO as its origin. We observed a similar effect in FixL which occurred with a 6 ps time constant (*18*).

The broad positive absorption spanning ~2050−2100 cm^{-1} (Figure 2A) during short delays was also observed by Afinrud et al. (*13*) and is attributed to heating of the chromophore by the pump pulse.

Docking Sites in P450BM3. X-ray diffraction studies of P450cam complexed with Xe have revealed the presence of several Xe cavities within the protein (*29*). Molecular dynamics studies confirm the existence of docking sites in the protein corresponding to the Xe sites (*26*), and CO photolysis studies of P450BM3 on the microsecond time scale suggest the occupancy of low-affinity sites for CO in the ferric (or possibly ferrous) protein (*30*). As P450 proteins retain a similar fold, it is conceivable that similar cavities exist in other P450s. A comparison of the sequences of P450BM3 and P450cam (shown in Figure S1 of the Supporting Information) reveals that the majority of residues lined with the Xe cavities in P450cam are either conserved or similar. We further performed a search for cavities in P450BM3 using CASTp (*38*) (polar hydrogens are excluded from the calculation, with a probe sphere radius of 2.5 Å) and found at least three cavities in the ground state protein structure. The cavities capable of accommodating CO molecules in P450BM3 appear to be clustered around residues corresponding to the residues lining up highly occupied cavities in P450cam, found by MD simulations of CO migration (*26*). The residues lining up the docking sites along helix I in P450cam are L244, V247, T252, L245, and G248 (*26*). The cavity found for P450BM3 involves A264 and T268, corresponding to G248 and T252 in P450cam (*26*), and might be a docking site for the dissociated CO (see Figure 3 for a schematic representation of the cavities in P450).

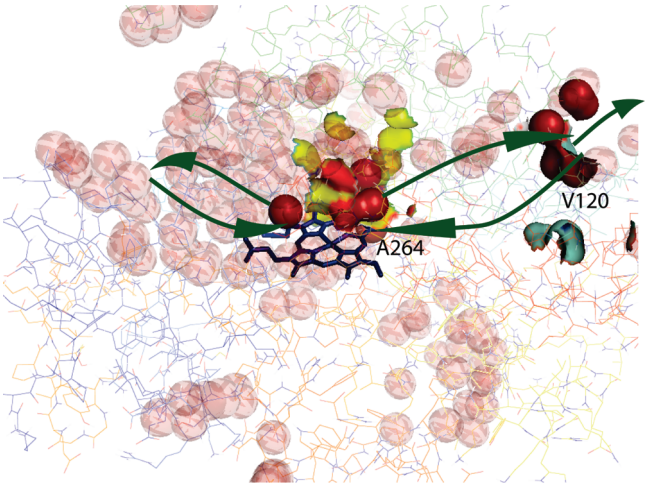

FIGURE 3: Schematic representation of the putative docking sites found in P450BM3. The spheres represent residues lining the cavities. Residues represented as surface correspond to residues in P450cam lining up xenon cavities. The pathways of CO within the protein are denoted with arrows.

The reaction course can now be summarized. The CO ligands are photodissociated instantaneously, and vibrational cooling of the ferrous deligated ground state takes place in 4 ps. As we do not observe geminate recombination in the mid-IR before 1 ns, the CO ligands are stored within the protein matrix in docking sites. In the initial high-energy regime, dissociated CO exists in two configurations with different oscillator strengths that are reduced in 1 ps, possibly due to a structural relaxation of the heme and/or protein. We identify by a cavity search algorithm docking sites that may be related to the Xe binding cavities found in P450cam.

ACKNOWLEDGMENT

We thank anonymous reviewers for valuable comments about the work. We thank Henny van Roon for the expression and purification of P450BM3.

SUPPORTING INFORMATION AVAILABLE

Comparison of the sequences of P450BM3 and P450cam (Figure S1). This material is available free of charge via the Internet at http://pubs.acs.org.

REFERENCES

(1) Nelson, D. R., Koymans, L., Kamataki, T., Stegeman, J. J., Feyereisen, R., Waxman, D. J., Waterman, M. R., Gotoh, O., Coon, M. J., Estabrook, R. W., Gunsalus, I. C., and Nebert, D. W. (1996) P450 superfamily: Update on new sequences, gene mapping, accession numbers and nomenclature. *Pharmacogenetics 6* (1), 1–42.

(2) Greengar, P., Psychoyo, S., Tallan, H. H., Cooper, D. Y., Rosentha, O., and Estabroo, W. (1967) Aldosterone synthesis by adrenal mitochondria. 3. Participation of Cytochrome P-450. *Arch. Biochem. Biophys. 121* (2), 298.

(3) Remmer, H., Schenkma, J., Estabroo, Rw., Sasame, H., Gillette, J., Narasimh, S., Cooper, D. Y., and Rosentha, O. (1966) Drug interaction with hepatic microsomal cytochrome. *Mol. Pharmacol. 2* (2), 187.

(4) Werck-Reichhart, D., and Feyereisen, R. (2000) Cytochromes P450: A success story. *Genome Biol. 1* (6), reviews3003.1–reviews3003.9.

(5) Ortiz de Montellano, P. R. (1995) Cytochrome P-450: Structure, Mechanism, and Biochemistry , 2nd ed., Plenum Publishing Corp., London.

(6) Murakami, K., and Mason, H. S. (1967) An Electron Spin Resonance Study of Microsomal Fex. *J. Biol. Chem. 242* (6), 1102–1110.

(7) Poulos, T. L. (1996) The role of the proximal ligand in heme enzymes. *JBIC, J. Biol. Inorg. Chem. 1* (4), 356–359.

(8) Narhi, L. O., and Fulco, A. J. (1986) Characterization of a catalytically self-sufficient 119,000-dalton cytochrome P-450 monooxygenase induced by barbiturates in *Bacillus megaterium*. *J. Biol. Chem. 261* (16), 7160–7169.

(9) Narhi, L. O., and Fulco, A. J. (1987) Identification and characterization of 2 functional domains in Cytochrome-P-450BM-3, a catalytically self-sufficient monooxygenase induced by barbiturates in *Bacillus megaterium*. *J. Biol. Chem. 262* (14), 6683–6690.

(10) Noble, M. A., Miles, C. S., Chapman, S. K., Lysek, D. A., Mackay, A. C., Reid, G. A., Hanzlik, R. P., and Munro, A. W. (1999) Roles of key active-site residues in flavocytochrome P450 BM3. *Biochem. J. 339*, 371–379.

(11) Ravichandran, K. G., Boddupalli, S. S., Hasemann, C. A., Peterson, J. A., and Deisenhofer, J. (1993) Crystal structure of hemoprotein domain of P450BM-3, a prototype for microsomal P450S. *Science 261* (5122), 731–736.

(12) Pylypenko, O., and Schlichting, I. (2004) Structural aspects of ligand binding to and electron transfer in bacterial and fungal P450S. *Annu. Rev. Biochem. 73* (1), 991–1018.

(13) Anfinrud, P. A., Hann, C., and Hochstrasser, R. M. (1989) Direct observations of ligand dynamics in hemoglobin by subpicosecond infrared spectroscopy. *Proc. Natl. Acad. Sci. U.S.A. 86* (21), 8387–8391.

(14) Austin, R. H., Beeson, K. W., Eisenstein, L., Frauenfelder, H., and Gunsalus, I. C. (1975) Dynamics of ligand binding to myoglobin. *Biochemistry 14* (24), 5355–5373.

(15) Lim, M., Jackson, T. A., and Anfinrud, P. A. (1993) Nonexponential protein relaxation: Dynamics of conformational change in myoglobin. *Proc. Natl. Acad. Sci. U.S.A. 90* (12), 5801–5804.

(16) Lim, M. H., Jackson, T. A., and Anfinrud, P. A. (1997) Modulating carbon monoxide binding affinity and kinetics in myoglobin: The roles of the distal histidine and the heme pocket docking site. *JBIC, J. Biol. Inorg. Chem. 2* (4), 531–536.

(17) Petrich, J. W., and Martin, J. L. (1989) Ultrafast absorption and Raman spectroscopy of hemeproteins. *Chem. Phys. 131* (1), 31–47.

(18) van Wilderen, L. J. G. W., Key, J. M., Van Stokkum, I. H. M., van Grondelle, R., and Groot, M. L. (2009) Dynamics of carbon monoxide photodissociation in *Bradyrhizobium japonicum* FixL probed by picosecond midinfrared spectroscopy. *J. Phys. Chem. B 113* (11), 3292–3297.

(19) Kapetanaki, S. M., Field, S. J., Hughes, R. J. L., Watmough, N. J., Liebl, U., and Vos, M. H. (2008) Ultrafast ligand binding dynamics in the active site of native bacterial nitric oxide reductase. *Biochim. Biophys. Acta 1777* (7−8), 919–924.

(20) Vos, M. H. (2009) Ultrafast dynamics of ligands within heme proteins. *Biochim. Biophys. Acta* (in press).

(21) Lamb, D. C., Nienhaus, K., Arcovito, A., Draghi, F., Miele, A. E., Brunori, M., and Nienhaus, G. U. (2002) Structural Dynamics of Myoglobin. Ligand migration among protein cavities studied by Fourier transform infrared/temperature derivative spectroscopy. *J. Biol. Chem. 277* (14), 11636–11644.

(22) Tilton, R. F., Kuntz, I. D., and Petsko, G. A. (1984) Cavities in proteins: Structure of a metmyoglobin xenon complex solved to 1.9 Å. *Biochemistry 23* (13), 2849–2857.

(23) Nienhaus, K., Olson, J. S., Franzen, S., and Nienhaus, G. U. (2005) The origin of Stark splitting in the initial photoproduct state of MbCO. *J. Am. Chem. Soc. 127* (1), 40–41.

(24) Ruscio, J. Z., Kumar, D., Shukla, M., Prisant, M. G., Murali, T. M., and Onufriev, A. V. (2008) Atomic level computational identification of ligand migration pathways between solvent and binding site in myoglobin. *Proc. Natl. Acad. Sci. U.S.A. 105* (27), 9204–9209.

(25) Manho, L., Timothy, A. J., and Philip, A. A. (1995) Mid-infrared vibrational spectrum of CO after photodissociation from heme: Evidence for a ligand docking site in the heme pocket of hemoglobin and myoglobin. *J. Chem. Phys. 102* (11), 4355–4366.

(26) Mouawad, L., Tetreau, C., Abdel-Azeim, S., Perahia, D., and Lavalette, D. (2007) CO migration pathways in cytochrome P450cam studied by molecular dynamics simulations. *Protein Sci. 16* (5), 781–794.

(27) Cojocaru, V., Winn, P. J., and Wade, R. C. (2007) The ins and outs of cytochrome P450s. *Biochim. Biophys. Acta 1770* (3), 390–401.

(28) Hritz, J., de Ruiter, A., and Oostenbrink, C. (2008) Impact of plasticity and flexibility on docking results for cytochrome P450 2D6: A combined approach of molecular dynamics and ligand docking. *J. Med. Chem. 51* (23), 7469–7477.

(29) Wade, R. C., Winn, P. J., and Schlichting, I. (2004) Sudarko, a survey of active site access channels in cytochromes P450. *J. Inorg. Biochem. 98* (7), 1175–1182.

(30) Girvan, H. M., Seward, H. E., Toogood, H. S., Cheesman, M. R., Leys, D., and Munro, A. W. (2007) Structural and spectroscopic characterization of P450 BM3 mutants with unprecedented P450 heme iron ligand sets: New heme ligation states influence conformational equilibria in P450 BM3. *J. Biol. Chem. 282* (1), 564–572.

(31) McLean, M. A., Yeom, H., and Sligar, S. G. (1996) Carbon monoxide binding to cytochrome P450BM-3: Evidence for a substrate-dependent conformational change. *Biochimie 78* (8−9), 700–705.

(32) Marchal, S., Girvan, H. M., Gorren, A. C. F., Mayer, B., Munro, A. W., Balny, C., and Lange, R. (2003) Formation of transient oxygen complexes of cytochrome P450 BM3 and nitric oxide synthase under high pressure. *Biophys. J. 85* (5), 3303–3309.

(33) Lussenburg, B. M. A., Keizers, P. H. J., de Graaf, C., Hidestrand, M., Ingelman-Sundberg, M., Vermeulen, N. P. E., and Commandeur, J. N. M. (2005) The role of phenylalanine 483 in cytochrome P450 2D6 is strongly substrate dependent. *Biochem. Pharmacol. 70* (8), 1253–1261.

(34) Omura, T., and Sato, R. (1964) The Carbon Monoxide-binding Pigment of Liver Microsomes. I. Evidence for its hemoprotein nature. *J. Biol. Chem. 239* (7), 2370–2378.

(35) Groot, M. L., van Wilderen, L., and Di Donato, M. (2007) Time-resolved methods in biophysics. 5. Femtosecond time-resolved and dispersed infrared spectroscopy on proteins. *Photochem. Photobiol. Sci. 6* (5), 501–507.

(36) van Stokkum, I. H. M., Larsen, D. S., and van Grondelle, R. (2004) Global and target analysis of time-resolved spectra. *Biochim. Biophys. Acta 1657* (2−3), 82–104.

(37) Groot, M. L., Breton, J., van Wilderen, L. J. G. W., Dekker, J. P., and van Grondelle, R. (2004) Femtosecond visible/visible and visible/mid-IR pump-probe study of the Photosystem II core antenna complex CP47. *J. Phys. Chem. B 108* (23), 8001–8006.

(38) Dundas, J., Ouyang, Z., Tseng, J., Binkowski, A., Turpaz, Y., and Liang, J. (2006) CASTp: Computed atlas of surface topography of proteins with structural and topographical mapping of functionally annotated residues. *Nucleic Acids Res. 34*, W116–W118

(39) Cao, W., Christian, J. F., Champion, P. M., Rosca, F., and Sage, J. T. (2001) Water penetration and binding to ferric myoglobin. *Biochemistry 40* (19), 5728–5737

(40) Gao, Y., Koyama, M., El-Mashtoly, S. F., Hayashi, T., Harada, K., Mizutani, Y., and Kitagawa, T. (2006) Time-resolved Raman evidence for energy 'funneling' through propionate side chains in heme 'cooling' upon photolysis of carbonmonoxy myoglobin. *Chem. Phys. Lett. 429* (1−3), 239–243

(41) Henry, E. R., Eaton, W. A., and Hochstrasser, R. M. (1986) Molecular dynamics simulations of cooling in laser-excited heme proteins. *Proc. Natl. Acad. Sci. U.S.A. 83* (23), 8982–8986

(42) Lim, M., Jackson, T. A., and Anfinrud, P. A. (1996) Femtosecond near-IR absorbance study of photoexcited myoglobin: Dynamics of electronic and thermal relaxation. *J. Phys. Chem. 100* (29), 12043–12051.

(43) Contzen, J., and Jung, C. (1998) Step-scan time-resolved FTIR spectroscopy of cytochrome P-450cam carbon monoxide complex: A salt link involved in the ligand-rebinding process. *Biochemistry 37* (13), 4317–4324.

(44) Garczarek, F., Wang, J., El-Sayed, M. A., and Gerwert, K. (2004) The assignment of the different infrared continuum absorbance changes observed in the 3000−1800-cm^{-1} region during the bacteriorhodopsin photocycle. *Biophys. J. 87* (4), 2676–2682.
(45) Liebl, U., Lipowski, G., Negrerie, M., Lambry, J.-C., Martin, J.-L., and Vos, M. H. (1999) Coherent reaction dynamics in a bacterial cytochrome c oxidase. *Nature 401* (6749), 181–184.
(46) Petrich, J. W., Poyart, C., and Martin, J. L. (1988) Photophysics and reactivity of heme proteins: A femtosecond absorption study of hemoglobin, myoglobin, and protoheme. *Biochemistry 27* (11), 4049–4060.
(47) Vos, M. H. (2008) Ultrafast dynamics of ligands within heme proteins. *Biochim. Biophys. Acta 1777* (1), 15–31.
(48) Lim, M. H., Jackson, T. A., and Anfinrud, P. A. (1996) Femtosecond near-IR absorbance study of photoexcited myoglobin: Dynamics of electronic and thermal relaxation. *J. Phys. Chem. 100* (29), 12043–12051.
(49) Lian, T. Q., Locke, B., Kholodenko, Y., and Hochstrasser, R. M. (1994) Energy-flow from solute to solvent probed by femtosecond IR spectroscopy: Malachite green and heme protein solutions. *J. Phys. Chem. 98* (45), 11648–11656.
(50) Park, E. S., Andrews, S. S., Hu, R. B., and Boxer, S. G. (1999) Vibrational Stark spectroscopy in proteins: A probe and calibration for electrostatic fields. *J. Phys. Chem. B 103* (45), 9813–9817.
(51) Diane, E. S., John, E. S., Timothy, A. J., Manho, L., and Philip, A. A. (1999) Vibrational population relaxation of carbon monoxide in the heme pocket of photolyzed carbonmonoxy myoglobin: Comparison of time-resolved mid-IR absorbance experiments and molecular dynamics simulations. *Proc. Natl. Acad. Sci. U.S.A. 96* (25), 14324–14329.
(52) Rao, K. N., Ed. (1972) Molecular Spectroscopy: Modern Research , Academic Press, New York.
(53) Lim, M. H., Jackson, T. A., and Anfinrud, P. A. (1997) Ultrafast rotation and trapping of carbon monoxide dissociated from myoglobin. *Nat. Struct. Biol. 4* (3), 209–214.
(54) Meller, J., and Elber, R. (1998) Computer simulations of carbon monoxide photodissociation in myoglobin: Structural interpretation of the B states. *Biophys. J. 74* (2), 789–802.
(55) Ewing, G. E. (1962) Infrared spectra of liquid and solid carbon monoxide. *J. Chem. Phys. 37* (10), 2250–2256.
(56) Lim, M. H., Jackson, T. A., and Anfinrud, P. A. (1995) Midinfrared vibrational-spectrum of CO after photodissociation from heme: Evidence for a ligand docking site in the heme pocket of hemoglobin and myoglobin. *J. Chem. Phys. 102* (11), 4355–4366.
(57) Lim, M. H., Jackson, T. A., and Anfinrud, P. A. (1997) Ultrafast rotation and trapping of carbon monoxide dissociated from myoglobin. *Nat. Struct. Biol. 4* (3), 209–214.